Impact of *Mycobacterium tuberculosis* Glycolipids on the CD4$^+$ T Cell–Macrophage Immunological Synapse

Ivan Mwebaza,* Rachel Shaw,* Qing Li,* Shane Fletcher,* Jacqueline M. Achkar,† Clifford V. Harding,*,‡,1 Stephen M. Carpenter,*,‡,1 and W. Henry Boom*,‡,1

Mycobacterium tuberculosis **cell-wall glycolipids such as mannosylated lipoarabinomannan (ManLAM) can inhibit murine CD4$^+$ T cells by blocking TCR signaling. This results in suppression of IL-2 production, reduced T cell proliferation, and induction of CD4$^+$ T cell anergy. This study extended these findings to the interaction between primary human CD4$^+$ T cells and macrophages infected by mycobacteria. Exposure of human CD4$^+$ T cells to ManLAM before activation resulted in loss of polyfunctionality, as measured by IL-2, IFN-γ, and TNF-α expression, and reduced CD25 expression. This was not associated with upregulation of inhibitory receptors CTLA-4, PD-1, TIM-3, and Lag-3. By confocal microscopy and imaging flow cytometry, ManLAM exposure reduced conjugate formation between macrophages and CD4$^+$ T cells. ManLAM colocalized to the immunological synapse (IS) and reduced translocation of lymphocyte-specific protein tyrosine kinase (LCK) to the IS. When CD4$^+$ T cells and *Mycobacterium bovis* BCG–infected monocytes were cocultured, ManLAM colocalized to CD4$^+$ T cells, which formed fewer conjugates with infected monocytes. These results demonstrate that mycobacterial cell-wall glycolipids such as ManLAM can traffic from infected macrophages to disrupt productive IS formation and inhibit CD4$^+$ T cell activation, contributing to immune evasion by *M. tuberculosis*.** ***The Journal of Immunology*****, 2023, 211: 1385–1396.**

Development of a better vaccine and immunotherapeutics against tuberculosis (TB) has been hampered by inadequate understanding of the interactions between *Mycobacterium tuberculosis*, macrophages, and T cells. Upon inhalation of aerosols, *M. tuberculosis* bacilli are taken up by lung APCs that process and present their Ags to cells of the adaptive immune response (1, 2). This cell-mediated immune response should facilitate clearance of the organism (3). However, *M. tuberculosis* is not cleared in many infected individuals, surviving in granulomas as a latent *M. tuberculosis* infection (LTBI) (4, 5) and in some progressing to active disease (6, 7). Immune evasion by *M. tuberculosis* allows it to resist macrophage killing and recognition of infected APCs by T cells (8).

MHC class II (MHC-II)-restricted CD4$^+$ T cells have a central role in the T cell response to *M. tuberculosis*. HIV-induced CD4$^+$ T cell depletion provides strong evidence for a dominant role of human CD4$^+$ T cells in controlling *M. tuberculosis* (9). Murine MHC-II knockout and nonhuman primate CD4$^+$ T cell depletion studies experimentally support the importance of CD4$^+$ T cells (10). CD4$^+$ T cells expressing IFN-γ, TNF-α, and IL-2 are associated with protective responses to *M. tuberculosis* (11). CD4$^+$ T cells from persons with LTBI recognize a diverse range of Ags (12), but because antigenic variation among *M. tuberculosis* strains is minimal, this likely is not a major mechanism of immune evasion.

Molecular mechanisms used by *M. tuberculosis* to resist innate immune responses include disruption of phagolysosome fusion and resisting of killing by superoxide, autophagy, and apoptosis (13). *M. tuberculosis* also indirectly and directly interferes with recognition of infected cells by CD4$^+$ T cells. *M. tuberculosis* lipoproteins activate TLR2 signaling in macrophages, which inhibits MHC-II Ag processing (5). *M. tuberculosis*'s secreted protein EsxH can interfere with T cell activation (14), and *M. tuberculosis*–infected dendritic cells can export Ags to uninfected cells as decoy for CD4$^+$ T cells (15). Our recent studies have focused on *M. tuberculosis* glycolipids, especially mannosylated lipoarabinomannan (ManLAM), as inhibitors of CD4$^+$ T cell activation. Through direct contact with infected cells or release of bacterial microvesicles, CD4$^+$ T cells are exposed to *M. tuberculosis* products, including lipids, proteins, and glycolipids such as ManLAM (16–19). ManLAM can directly inhibit CD4$^+$ T cells by blocking phosphorylation of proximal TCR kinases LCK, Zap70, and adaptor protein LAT, resulting in downregulation of IL-2 expression, hypoproliferation, and anergy through the induction of Gene Related to Anergy in Lymphocytes (16, 17, 19, 20).

Although a critical insight into *M. tuberculosis* pathogenesis, the discovery and dissection of the mechanism of *M. tuberculosis* glycolipid-mediated inhibition of CD4$^+$ T cell activation was performed in a murine experimental system (16, 17, 19, 20). In this study, we sought to determine the impact of ManLAM and mycobacterial infection on the interaction between human CD4$^+$ T cells and macrophages with a particular focus on the IS. Using primary human CD4$^+$ T cells, we determined the effect of ManLAM and *Mycobacterium bovis* BCG (BCG) infection on (1) CD4$^+$ T cell polyfunctionality, (2) conjugate formation between CD4$^+$ T cells and macrophages,

*Department of Medicine, Case Western Reserve University and University Hospitals Cleveland Medical Center, Cleveland, OH; †Department of Medicine, Albert Einstein College of Medicine, Bronx, NY; and ‡Department of Pathology, Case Western Reserve University, Cleveland, OH

[1]C.V.H., S.M.C., and W.H.B. are cosenior authors.

ORCIDs: 0000-0002-7521-3305 (I.M.); 0000-0003-3594-8638 (S.F.); 0000-0002-6333-162X (C.V.H.); 0000-0001-9879-327X (S.M.C.); 0000-0001-5760-9595 (W.H.B.).

Received for publication February 10, 2023. Accepted for publication August 24, 2023.

This work was supported by the National Institutes of Health (Grant D43TW010319 to I.M. and W.H.B.; Grant AI034343 to C.V.H.; Grant AI146329 to J.M.A.; Grant AI027243 to W.H.B.; and Contract 75N93019C00071 to W.H.B.) and the Cytometry and Imaging Microscopy of Shared Resource of the Case Comprehensive Center (P30CA043703).

Address correspondence and reprint requests to Ivan Mwebaza, Case Western Reserve University, 10900 Euclid Avenue, Cleveland, OH 44106. E-mail address: ixm141@case.edu

The online version of this article contains supplemental material.

Abbreviations used in this article: AF, Alexa Fluor; BCG, *Mycobacterium bovis* BCG; BCG/CFP, cyan fluorescent protein–expressing BCG; Cat#, catalog number; CFP, cyan fluorescent protein; IFC, imaging flow cytometry; IS, immunological synapse; LTBI, latent *Mycobacterium tuberculosis* infection; ManLAM, mannosylated lipoarabinomannan; MHC-II, MHC class II; MOI, multiplicity of infection; PFA, paraformaldehyde; rIL-2, recombinant human IL-2; SEB, staphylococcal enterotoxin B; TB, tuberculosis.

https://doi.org/10.4049/jimmunol.2300107

(3) the integrity of the IS, and (4) colocalization of ManLAM to $CD4^+$ T cells when cocultured with infected primary monocytes.

Materials and Methods

Ethics statement

Human $CD4^+$ T cell donors ($n = 12$) were recruited and consented under the study "Heterogeneity of $CD4^+$ T cells in *M. tuberculosis* infection" that was approved by the Institutional Review Board of University Hospitals Case Medical Center (IRB Number: 03-88-63). Normal $CD4^+$ T cells and monocytes were also obtained from three adult donors by leukapheresis from AllCells (Almeda, CA). In both cases, all samples were deidentified, and the study was conducted under the ethical principles as specified in the Declaration of Helsinki.

Abs

$CD4^+$ T cells were stimulated using mAbs anti-CD28 (catalog number [Cat#] 555725, CD28.2 clone; BD Biosciences) and anti-CD3ε (Cat#16-0037-81, OKT3 clone; eBioscience). The following mAbs were used for flow cytometric assays (unless otherwise stated, all Abs were mouse anti-human mAbs), anti–CD3-BUV395, anti–ICOS-BV711, anti–PD-1-BV650, anti–CTLA-4-BV421, anti–CD40L-PE-CF594, anti–Lag-3-allophycocyanin-R700, anti–IL-17A-BV421, anti–CD45RA-PE-CF594, anti–CD27-allophycocyanin, anti–IFN-γ-PE, anti–TNF-α-AF700 (Alexa Fluor 700), anti–IL-2-BV650, anti–CD25-BUV395, anti–CD69-BV421 (Cat# 564001, 563833, 564324, 565931, 563589, 565775, 562933, 565419, 558664, 559326, 557996, 563467, 567484, and 562883, respectively; BD Biosciences), anti–CD4-allophycocyanin-cy7, anti–TIM-3-PE/cy7, anti–CD28-FITC, anti–CD4-AF594 (Cat# 300518, 345014, 302906, and 300544, respectively; BioLegend). Aqua dye (BV510, Cat# L34965; ThermoFisher) was used for live-dead cell stain. Anti–CD3-AF488 (Cat# 300454; BioLegend), anti–CD14-PE (Cat# 562691; BD Biosciences), and anti–LCK-AF647 (Cat# SC-433; Santa Cruz Technologies) were used for imaging flow cytometry (IFC).

The following primary Abs were used for confocal microscopy: rabbit anti-CD4 recombinant monoclonal (Cat#MA5-32166; Invitrogen), mouse anti-LCK monoclonal (Cat# MA5-12303; Invitrogen), mouse anti-CD14 monoclonal (60004 [STEMCELL Technologies] or 557152 [BD Biosciences]; same clone: M5E2), rabbit anti-CD3 recombinant monoclonal (ab135372; Abcam), Mouse anti-CD86 monoclonal (Cat# 305435; BioLegend).

Human anti-ManLAM mAb (L1AM04) was isolated from PBMCs from an individual with LTBI via single B cell sorting with delipidated ManLAM glycan arabinomannan (21). This mAb was generated by cloning L1AM04's H and L chain V regions into human IgG1 H and L chain expression vectors followed by coexpression in 293 HEK cells and provided by Dr. J. Achkar (Albert Einstein College of Medicine). L1AM04 is distinct from other anti-ManLAM mAbs and reacts specifically with the ManLAM cap component Man_3Ara4 [reviewed by Corrigan et al. (22)]. It binds to various laboratory and clinical *M. tuberculosis* strains, as well as BCG, and recognizes *M. tuberculosis* and ManLAM in the lungs of *M. tuberculosis*–infected mice (21). Goat anti-Mouse IgG-AF488 (Cat# A11001; Invitrogen), goat anti-Rabbit IgG-AF594 (Cat# A11012; Invitrogen), and goat anti-human IgG-AF647 (Cat# A21445; ThermoFisher) were used as secondary Abs.

Reagents

ManLAM was provided by BEI Resources (NR-14848). In brief, the glycolipid was purified from the cell wall of the irradiated *M. tuberculosis* H37Rv strain by delipidation, ethanol precipitation, and size exclusion chromatography. The lyophilized glycolipid was resuspended in 1× PBS at 1 μg/μl, sonicated, aliquoted, and stored at −80°C.

Ammonium chloride, calcium chloride, and sucrose (Cat# A4514, C-7902, and S5016, respectively) were purchased from Sigma-Aldrich (St. Louis, MO). Paraformaldehyde (PFA) was purchased from Electron Microscopy Sciences (Hatfield, PA). Recombinant human IL-2 (rIL-2; Cat#200-02) was purchased from PeproTech (Granbury, NJ).

BCG Connaught (35745; ATCC, Manassas, VA) was grown as described in Li et al. (23). In brief, BCG was grown in Middlebrook 7H9 medium (BD Diagnostics) supplemented with 10% albumin-dextrose-catalase (Difco, Detroit, MI) and glycerol (6% v/v). Cyan fluorescent protein–expressing BCG (BCG/CFP) was made by transformation with plasmid pDH3 (Yeast Resource Center, University of Washington, WA) and cloned into pMV262 as described previously (24, 25).

Isolation of $CD4^+$ T cells

$CD4^+$ T cells were enriched from peripheral blood obtained from healthy donors or from commercially sourced leukapheresis donors. In both cases, PBMCs were isolated by density gradient-centrifugation method using Ficoll Paque Plus. Total $CD4^+$ T cells were enriched by immunomagnetic negative selection using EasySep Human $CD4^+$ T cell enrichment kit (Cat# 19052; STEMCELL Technologies). The average purity was 97–98%. $CD4^+$ T cells were rested overnight in RPMI1640 media (Cat# 12167Q; Lonza Bio Whittaker) supplemented with 0.1 mM nonessential amino acids (Cat# BW13-114E; Fisher Scientific), 2 mM L-glutamine (Cat# BW17-605E; Fisher Scientific), 1 μg/ml penicillin/streptomycin (Cat# 17-602E; Lonza), 1 mM sodium pyruvate (Cat# BW13-115E; Fisher Scientific), 10% heat-inactivated FBS (Cat #100-106; Gemini Bio), 4 μl/l 2-ME (Cat# M3148; Millipore Sigma), and 0.2 M HEPES buffer (Cat# 17-737E; Fisher Scientific) (complete media, hereafter referred to as M10), or in chemically predefined X-VIVO15 media (with L-glutamine, gentamicin, and phenol red; Cat# 04-418Q; Lonza Bioscience).

Isolation of peripheral blood monocytes

Primary human monocytes were isolated from PBMCs by negative selection using EasySep isolation kit (Cat# 19359; STEMCELL Technologies) and were rested in antibiotic-free M10 for 24 h at 1×10^6 cells/ml before use. The average purity was 96–99%.

Activation of THP-1 cells

THP-1 cells that had undergone <10 passages were stimulated with 200 ng/ml IFN-γ (Cat#570206; BioLegend) in M10 in suspension for 24 h. The average fold increase in HLA-DR expression by THP-1 cells after IFN-γ activation was 5-fold, as measured by flow cytometry.

Exposure of $CD4^+$ T cells to ManLAM

ManLAM aliquots (1 μg/μl, 40 μl) were thawed and sonicated for 25 min to emulsify the micelles. $CD4^+$ T cells were incubated with the glycolipid at 40 μg/ml in X-VIVO15 or M10 media for 1 h at 37°C, with rotary shaking. More than 95% of $CD4^+$ T cells acquired ManLAM on their surface as measured by flow cytometry (Supplemental Fig. 1).

Activation of $CD4^+$ T cells

For flow cytometric and ELISA assays, $CD4^+$ T cells were rested in X-VIVO15 medium at 1×10^6 cells/ml in culture flasks in a 37°C, 5% CO_2, humidified incubator overnight. The following day, $CD4^+$ T cells were recounted, washed, and exposed to ManLAM in fresh X-VIVO15 medium for 1 h at 37°C on a rotating shaker. Cells were then activated by plate-bound anti-CD3ε (1 μg/ml) with or without soluble anti-CD28 (1 μg/ml) at 1×10^6 cells/ml in 24-well plates for 24 or 48 h. After stimulation, supernatants were collected for ELISA, and cells were stained for flow cytometric analysis of surface markers. For intracellular cytokine staining assays, cell protein transport inhibitor brefeldin A (Cat# 555029; BD Biosciences) was added at 1 μg/ml media, and cells were activated for 24 h before staining for flow cytometry.

Infection of peripheral blood monocytes with BCG

Monocytes rested in antibiotic-free M10 for 24 h were infected in fresh media with CFP-labeled or wild-type BCG that had been grown to OD of 0.4–8 in 7H9 medium, at multiplicity of infection (MOI) 1:1 or 5:1 for 48 h in 24-well plates. Cultures were monitored for cell viability and changes in color of the media. Cells were washed to remove uninternalized bacteria before downstream assays.

Intracellular cytokine staining and surface marker staining for flow cytometry

A total of 1×10^6 cells per condition were stained for surface markers and fixed with 1% PFA before acquisition. For intracellular cytokine staining, 1×10^6 cells per condition were stained using the BD Cytofix/Cytoperm Fixation/Permeabilization kit (Cat# 554714; BD) following manufacturer's instructions before 1% PFA fixation and acquisition. Cells were acquired on LSR Fortessa flow cytometer using BD FACSDiva software, and data were analyzed using FlowJo software (version 10).

ELISA assays

IL-2, IFN-γ, and TNF-α ELISA were performed using ELISA kits (Cat# 88-7025-88, Cat# 88-7346-88, and Cat# KHC4021; ThermoFisher Scientific) according to the manufacturer's instructions. Plates were read on a BioTek plate reader (Highland Park, VT) at wavelength 450 nm.

Analysis of LCK polarization by confocal microscopy

$CD4^+$ T cells rested in M10 media were exposed to ManLAM and cultured on anti-CD3ε–coated (3 μg/ml) poly-L-lysine–pretreated glass slides (Cat#22247; Polysciences) for 5 min at 37°C in 5% CO_2. They were then fixed with 3% PFA, permeabilized with 1% BSA/0.1% Tx-100 for 1 min, blocked with 1% BSA for 30 min, and then stained with rabbit anti-CD4 and mouse anti-LCK

mAbs for 3 h at room temperature, followed by secondary goat anti-mouse IgG-AF488 and goat anti-rabbit IgG-AF594. Slides were mounted in ProLong Diamond Antifade mounting medium (Cat# P36970; Fisher Scientific) before imaging under 60× oil immersion on Hyvolution SP8 confocal microscope (Leica Microsystems). Images were analyzed and processed in Leica Application Suite X (version 3.7.4.23463) and ImageJ software.

T cell–macrophage conjugate analysis by flow cytometry

IFN-γ–activated THP-1 cells were labeled with viability compatible CMFDA dye (Cat# C7025; Thermo Scientific) at 5 μM and then loaded with staphylococcal enterotoxin B (SEB) (Item No. BT202; Toxin Technology) at 5 μg/ml for 30 min. $CD4^+$ T cells were labeled with 0.5 μM viability compatible Deep red dye (Cat# C34565; Thermo Scientific) and then exposed to ManLAM as described earlier in RPMI 1640 media. Each cell type was washed and resuspended in M10 at 50,000 cells/μl. Resuspended cells were cocultured for 30 min at 37°C in 5% CO_2 by adding 10 μl of each cell type in a 96-well U-bottom plate. Cells then were fixed in 3% PFA and 3% sucrose in 1× PBS before acquisition on an LSR Fortessa flow cytometer. At least 50,000 events were acquired per condition.

T cell–macrophage conjugate analysis by IFC

$CD4^+$ T cells were exposed to ManLAM in RPMI 1640 media as described earlier. IFN-γ–activated THP-1 cells were loaded with SEB at 5 μg/ml for 30 min. Each cell type was washed and resuspended at 50,000 cells/μl in RPMI 1640 supplemented with 6 mM calcium chloride ($CaCl_2$). $CD4^+$ T cells and THP-1 cells were then coincubated at a ratio of 1:1 (4×10^6 cells in total) for 30 min at 37°C in 5% CO_2 in a 96-well U-bottom plate. Cells were then fixed with 2% PFA for 20 min at 4°C. PFA was neutralized by adding 100 mM ammonium chloride (NH_4Cl) for 20 min at room temperature. Cocultures of $CD4^+$ T cells and THP-1 cells were then resuspended in 200 μl staining buffer (10% FBS, 0.1% Triton X-100 in 1× PBS) for 10 min on ice. Cells were then stained for CD3, LCK, and CD14 for 40 min on ice and washed twice with wash buffer (5% BSA, 1% FBS in 1× PBS) before resuspension in fixation solution. A drop of Hoechst 33342 (Cat# R37605; Fisher Scientific) was added before acquisition. The cells were acquired on an ImageStream imaging flow cytometer (Amnis ImageStream; Luminex, Austin, TX), with 40× magnification at low-flow rate using INSPIRE software. Brightfield channels 01 and 09 and scattering channel 06 were acquired alongside fluorescence channels. Lasers 488, 405, 658 (fluorescence), and 785 (side scatter) were activated for acquisition. The bright-field background intensities were set at 740 for each camera. Approximately 30,000 events were acquired for each sample. Data files were analyzed using IDEAS software version 6.2.187 (Amnis; EMD Millipore, Seattle, WA). A conjugate was considered as an event with bright field, Hoechst (DAPI) was positive for two nuclei, and these nuclei were either CD3 or CD14 masked, with minimum aspect ratio of 0.6 for each of the CD3 and CD14 masks. A valley mask applied between the two nuclei was used to define the synapse of the conjugate. Two feature derivatives were used to determine the redistribution of LCK toward the synapse: (1) percentage of total LCK (as a function of intensity) that redistributed in the valley mask, and (2) a ratio of the brightest (maximum) pixel of LCK in the valley mask to the mean brightness of all LCK pixels in the conjugate.

Monocytes infected with CFP-labeled BCG (MOI 1:1) were cocultured with autologous $CD4^+$ T cells in the ratio of 1:1 for 72 h in a 24-well plate. Cells were afterward lifted off the plate using cell dissociation solution TrypLE select (Cat#12563011; Life Technologies), after which they were resuspended in RPMI 1640 media supplemented with 6 mM $CaCl_2$, with 5 μg/ml SEB, and then coincubated for 30 min at 37°C, 5% CO_2. Medium was removed, and pellets were incubated for >30 min. The cells were fixed with 2% PFA at 4°C, which was afterward neutralized with 100 mM NH_4Cl for 20 min at room temperature. Cells were then stained for CD3 and CD14 and acquired on ImageStream imaging flow cytometer and analyzed with IDEAS software as described earlier.

ManLAM colocalization toward the IS by confocal microscopy

$CD4^+$ T cells were incubated with ManLAM in RPMI 1640 media. IFN-γ activated THP-1 cells were loaded with SEB as previously described. Each cell type was resuspended at 50,000 cells/μl in RPMI 1640 media supplemented with 6 mM $CaCl_2$. $CD4^+$ T cells and THP-1 cells were then coincubated at a ratio of 1:1 (4×10^6 cells in total) for 30 min at 37°C in 5% CO_2 in a 96-well U-bottom plate. Cocultures were then layered on poly-L-lysine–treated glass slides for 15 min at 37°C; fixed with 3% PFA; and stained with rabbit anti-CD3, mouse anti-CD14, and human anti-ManLAM mAb, followed by goat anti-rabbit-AF594, goat anti-mouse AF488, and goat anti-human AF647 as secondary Abs. Slides were read and images processed as previously described. $CD4^+$ T cells cocultured with primary monocytes infected with wild-type BCG (MOI 5:1) as described earlier were also analyzed by confocal microscopy for acquisition of ManLAM onto their cell membranes and its colocalizing toward the IS. After incubation, the cells were layered on poly-L-lysine–treated glass slides at 37°C for 15 min. They were then stained for CD3 and ManLAM using the same primary and secondary Abs as described previously. To determine ManLAM colocalization to the IS, in some experiments, cocultures were incubated with SEB for 1 h before staining for CD3, CD86, and ManLAM. The slides were also imaged under 60× oil immersion, and images were processed with the same software packages as previously stated.

Statistical analysis

Prism (version 9.2.0; GraphPad, La Jolla, CA) was used to analyze the data. Unless otherwise stated, one-tailed paired *t* test was used to analyze comparisons across experimental conditions, and $p < 0.05$ was considered significant ($*p \leq 0.05$, $**p \leq 0.01$, and $***p \leq 0.001$). Differences between or ratios of paired values were considered consistent. In some experiments, Wilcoxon matched pairs signed rank test was used to compare outcomes across different donors of $CD4^+$ T cells ($*p \leq 0.05$, $**p \leq 0.01$, $***p \leq 0.001$, $****p \leq 0.0001$, and p^{ns} = not significant).

Results

ManLAM inhibits IL-2, TNF-α, and IFN-γ production by activated primary $CD4^+$ T cells without affecting T cell–inhibitory and costimulatory molecule expression

We adapted a protocol used to study the effect of *M. tuberculosis* glycolipids on the activation of murine polyclonal $CD4^+$ T cells to determine the extent to which ManLAM inhibits human $CD4^+$ T cell activation (20). Resting total $CD4^+$ T cells were purified by negative selection from PBMCs from healthy adults. Purified $CD4^+$ T cells were then exposed to 40 μg/ml ManLAM or medium alone for 1 h at 37°C before stimulation with plate-bound anti-CD3ε and soluble anti-CD28 for 24 or 48 h for assessment of intracytoplasmic cytokine staining in the presence of brefeldin A (1 μg/ml) and cytokine secretion by ELISA. IL-2, TNF-α, and IFN-γ secretion was significantly reduced when $CD4^+$ T cells were incubated with ManLAM before stimulation (Fig. 1A). These findings were confirmed and extended by flow cytometry, which revealed decreased intracellular IL-2, TNF-α, and IFN-γ expression as single cytokines (Fig. 1B, 1C) and in terms of polyfunctionality as decreased IL-2 together with IFN-γ or TNF-α (Fig. 1D). Anti-CD3ε without anti-CD28 served as control for suboptimal T cell activation and as comparator for the inhibitory effect of ManLAM pretreatment on human $CD4^+$ T cell activation. Taken together, these findings show human $CD4^+$ T cells are susceptible to ManLAM-mediated inhibition.

We next determined whether decreased cytokine production of T cells pretreated with ManLAM was related to changes in inhibitory or costimulatory molecule expression. As shown in Supplemental Fig. 2, ManLAM pretreatment had no effect on the expression of inhibitory receptors CTLA-4, PD-1, TIM-3, and Lag-3, or of costimulatory molecules CD40L and ICOS by $CD4^+$ T cells when compared with untreated cells. These results extend our earlier findings with Ag-specific murine $CD4^+$ T cells that exposure to ManLAM inhibits their activation as measured by reduced ability to produce cytokines without affecting T cell–inhibitory and costimulatory molecule expression (17).

ManLAM downregulates the coexpression of CD25 and CD69 by $CD4^+$ T cells, and addition of IL-2 does not reverse ManLAM-mediated inhibition

Next, we determined whether addition of exogenous IL-2 would reverse ManLAM's inhibitory effect. First, we measured the effect of ManLAM on expression of CD25 and CD69, two early T cell activation markers. $CD4^+$ T cells were exposed to ManLAM as described earlier and stimulated with plate-bound anti-CD3ε and soluble anti-CD28 for 24 h. ManLAM reduced coexpression of CD25 and CD69 by flow cytometry (Fig. 2A, 2B). On further

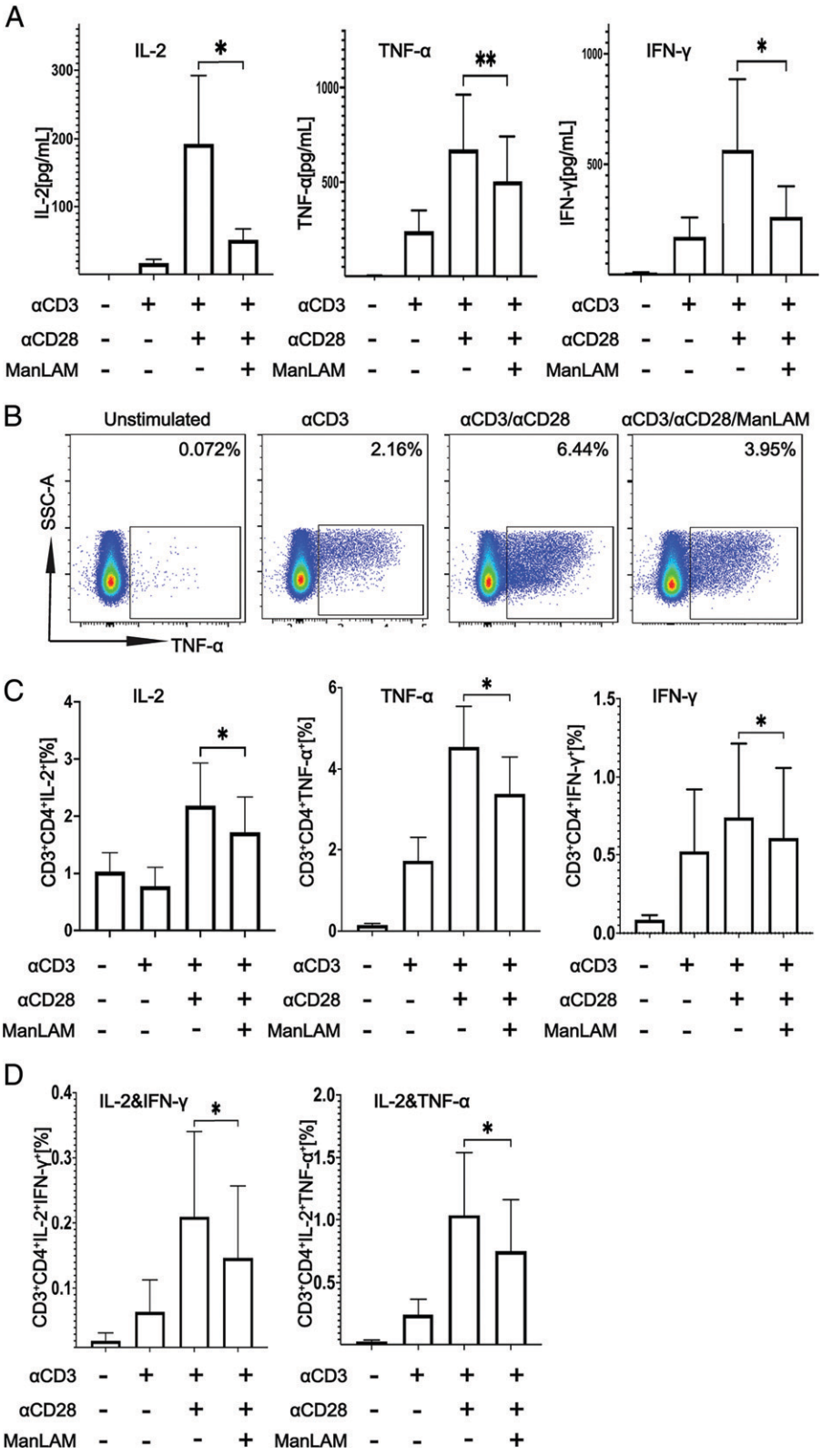

FIGURE 1. ManLAM inhibits the activation of human $CD4^+$ T cells. Purified human $CD4^+$ T cells were incubated with or without ManLAM (40 μg/ml) for 1 h. $CD4^+$ T cells were cultured in medium alone or stimulated with either plate-bound anti-CD3ε alone or together with soluble anti-CD28 (both at 1 μg/ml) for 24 or 48 h. (**A**) IL-2, TNF-α, and IFN-γ were measured in 48-h culture supernatants by ELISA. Data are the mean of two replicates for a total of three experiments from three different donors for IL-2 and TNF-α and four experiments from four donors for IFN-γ. (**B**) Percentages of cytokine-positive $CD4^+$ T cells by flow cytometry after 24-h stimulation in the presence of 1 μg/ml brefeldin A are shown for a representative experiment of six from six different donors. (**C**) Summary of percentage of cells expressing IL-2, TNF-α, and IFN-γ for six experiments from six different donors is shown. (**D**) Percentage of cells coexpressing IL-2 and TNF-α or IFN-γ by Boolean gating is shown for six experiments from six different donors. Data in (A), (C), and (D) are represented as mean ± SEM (*$p \leq 0.05$, **$p \leq 0.01$).

analysis, we observed this reduction in coexpression to be driven by CD25, because there was no statistically significant difference in CD69 expression between ManLAM-exposed and unexposed $CD4^+$ T cells (Fig. 2C, Supplemental Fig. 3A–C). By using changes in expression of CD25 and TNF-α as surrogates for ManLAM's effect, we determined whether addition of exogenous IL-2 would reverse the inhibition. $CD4^+$ T cells were stimulated with plate-bound anti-CD3ε and soluble anti-CD28 for 24 h, in the presence or absence of rIL-2 (10 ng/ml). Cells were stained for CD4, CD69, and CD25 and analyzed by flow cytometry. Supernatants were collected for TNF-α ELISA. IL-2 did not reverse the effects of ManLAM on CD25 and TNF-α expression (Fig. 2D, 2E). Addition of rIL-2 to T cells unexposed to ManLAM significantly increased expression of TNF-α (Fig. 2E). Decreased expression of CD25 by

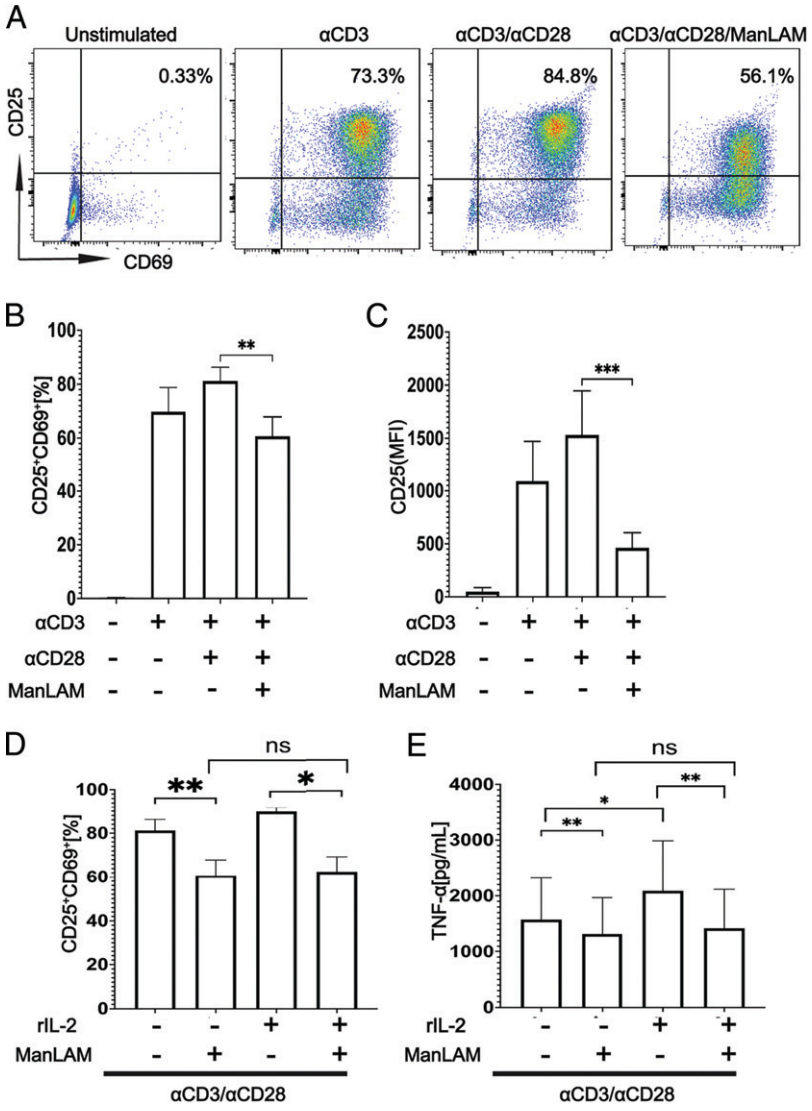

FIGURE 2. ManLAM downregulates CD25 and CD69 coexpression by human $CD4^+$ T cells, and addition of rIL-2 does not reverse their ManLAM-mediated inhibition. Purified human $CD4^+$ T cells were incubated with or without ManLAM (40 μg/ml) for 1 h. $CD4^+$ T cells were cultured in medium alone or stimulated with either plate-bound anti-CD3ε alone or together with soluble anti-CD28 (both at 1 μg/ml) for 24 h. Cells were then stained for CD4, CD69, and CD25 and analyzed by flow cytometry. (**A**) Flow cytometric graphs of CD25 and CD69 coexpression across four experimental conditions from a representative experiment of four from three donors. (**B**) Summary of CD25 and CD69 coexpression by $CD4^+$ T cells for four experiments from three donors. (**C**) Summary of CD25 median fluorescence intensity (MFI) for four experiments from three donors. Data in (B) and (C) are represented as mean ± SEM ($^{**}p \leq 0.01$, $^{***}p \leq 0.001$). (**D** and **E**) Purified human $CD4^+$ T cells were incubated with or without ManLAM (40 μg/ml) for 1 h. $CD4^+$ T cells then were stimulated with plate-bound anti-CD3ε and soluble anti-CD28 for 24 h, in the presence or absence of rIL-2 (10 ng/ml). Cells were then stained for CD4, CD69, and CD25 and analyzed by flow cytometry. Supernatants were collected for TNF-α by ELISA. (D) Summary data of impact of rIL-2 on CD25 and CD69 coexpression by $CD4^+$ T cells of four experiments from three donors. (E) Summary data of impact of rIL-2 on TNF-α secretion measured by ELISA from four experiments from three donors. Data in (D) and (E) are represented as mean ± SEM ($^*p \leq 0.05$, $^{**}p \leq 0.01$).

ManLAM, with no effect on CD69, and failure of IL-2 to reverse this inhibition suggests disruption of the TCR/IL-2R signaling axis leading to suboptimal activation of the cells.

ManLAM inhibits conjugate formation between $CD4^+$ T cells and THP-1 macrophages and reduces translocation of LCK toward the activation interface of $CD4^+$ T cells

Having determined that ManLAM inhibits T cell activation and cytokine production without inducing inhibitory receptor expression, we next focused on the impact of *M. tuberculosis* glycolipids on the interaction between $CD4^+$ T cells and macrophages, i.e., the IS. An artificial activation platform (pseudo-APC) was created by coating glass slides with anti-CD3ε and adding ManLAM-exposed or unexposed $CD4^+$ T cells for 5 min. Cells on slides were then fixed and stained for LCK and CD4, followed by confocal microscopy. Preincubation of $CD4^+$ T cells with ManLAM reduced polarization of LCK toward the artificial activation interface compared with ManLAM unexposed T cells (Fig. 3A, 3B).

To determine the effect of ManLAM on the formation of conjugates between $CD4^+$ T cells and THP-1 macrophages, we stimulated THP-1 cells for 24 h with IFN-γ before labeling with cell-tracking CMFDA dye. The labeled THP-1 cells were then treated with SEB to bind to MHC-II, allowing them to engage with Vβ-chain–expressing T cells. SEB-treated THP-1 cells were then cocultured for 30 min with ManLAM-exposed and unexposed Deep red dye–labeled $CD4^+$ T cells to allow for TCR–MHC-II crosslinking. Cocultured cells were analyzed by flow cytometry to determine CMFDA-Deep red dye (double-positive) events, i.e., $CD4^+$ T cell–THP-1 conjugates. As shown in Fig. 3C–E, ManLAM-exposed $CD4^+$ T cells formed fewer conjugates compared with nonexposed ones. These data suggest IS disruption as a contributing factor to ManLAM-mediated T cell inhibition.

To more definitively evaluate conjugate formation and the nature of the IS between $CD4^+$ T cells and SEB-loaded THP-1 cells, we used IFC. IFC integrates quantitative image acquisition and analysis, and thus the ability to interrogate morphological changes and quantitative translocation of proteins within cellular regions at individual cell and population levels (26–28). IFC was used not only to detect true $CD4^+$ T cell–THP-1 conjugates but also to measure differences in LCK localization to the IS in $CD4^+$ T cells exposed or unexposed to ManLAM. For these experiments we used the same experimental design as used for experiments described in Fig. 3C–E, i.e., coculture of SEB-loaded THP-1 and $CD4^+$ T cells. Supplemental Fig. 4B shows the IFC gating strategy. CD14 and DAPI (Hoechst) were used to identify THP-1 cells, and CD3 and DAPI were used to identify $CD4^+$ T cells. Initial gating selected CD14 and CD3 double-positive events. To exclude double-positive events with more than one THP-1 or more than one $CD4^+$ T cell, we gated on events with aspect ratios >0.6 for

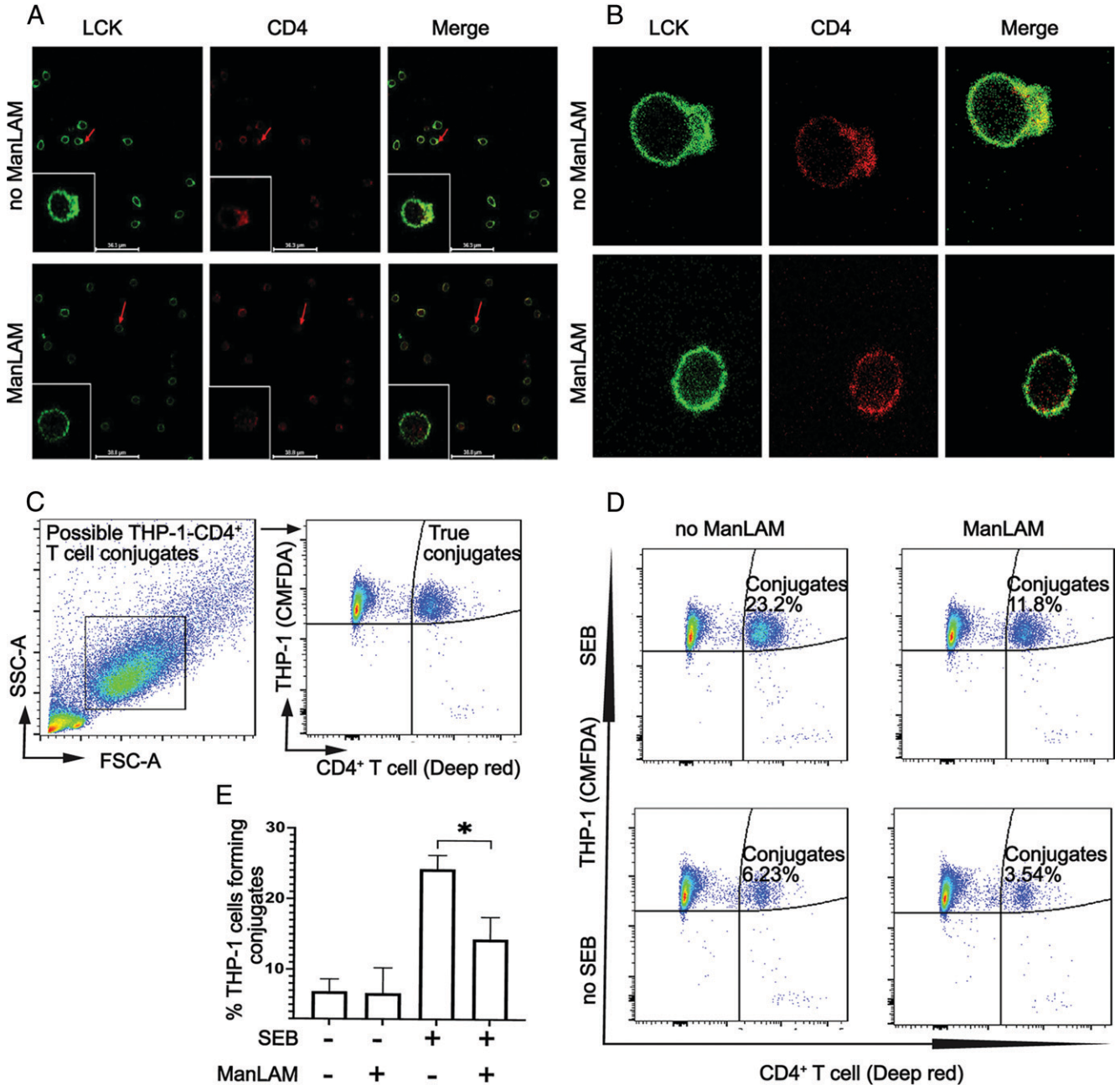

FIGURE 3. ManLAM blocks the mobilization of LCK toward the activation interface and inhibits the formation of conjugates between $CD4^+$ T cells and THP-1 cells. (**A** and **B**) Purified human $CD4^+$ T cells were incubated with or without ManLAM (40 μg/ml) for 1 h. T cells then were cultured on anti-CD3ε (3 μg/ml)-coated slides for 5 min, fixed, permeabilized, and stained with primary mouse anti-LCK and rabbit anti-CD4. This was followed with secondary AF488-conjugated goat anti-mouse IgG and AF594-conjugated goat anti-rabbit IgG. Fixed cells were imaged under 60× oil immersion by confocal microscopy. (A) Representative images for one of two experiments from two donors of $CD4^+$ T cells are shown. (B) Enlarged images of two $CD4^+$ T cells, one exposed and another unexposed to ManLAM before incubation on anti-CD3ε-coated slides. Images are representative of one of two experiments from two donors. (**C**–**E**) THP-1 macrophages were stimulated with IFN-γ (200 ng/ml) for 24 h. Macrophages were labeled with viability-compatible CMFDA dye and loaded with 5 μg/ml SEB for 30 min. Cells were washed and cocultured with human $CD4^+$ T cells that had been labeled with viability-compatible Deep red dye and incubated with or without ManLAM (40 μg/ml) for 1 h. $CD4^+$ T cells and THP-1 cells were cocultured at a ratio of 1:1 for 30 min at 37°C in 5% CO_2 before analysis by flow cytometry. (C) The gating strategy used to evaluate $CD4^+$ T cell–THP-1 conjugates by flow cytometry is representative of four experiments from four donors. (D) Flow cytometry graphs from a single representative experiment of four from four donors demonstrating the detection of conjugates across four experimental conditions. (E) Summary results for four experiments from four donors showing percentage of conjugates formed across the experimental conditions (mean ± SEM, paired *t* test, $*p \leq 0.05$).

either CD3 or CD14 masks. This allowed focusing on double-positive events of single $CD3^+$ and $CD14^+$ cells. Using this approach, we first compared the rates of conjugate formation between ManLAM-pretreated and nontreated $CD4^+$ T cells cocultured with SEB-loaded THP-1 cells. We found decreased numbers of $CD3^+CD14^+$ dual-positive conjugate events when $CD4^+$ T cells were pretreated with ManLAM (Fig. 4A). Fig. 4B shows representative images demonstrating that true $CD4^+$ T cell–THP-1 conjugates were detected by IFC. Fig. 4C summarizes the results of four experiments showing a 23% reduction in $CD4^+$ T cell–THP-1 conjugate formation when T cells were pretreated with ManLAM. These IFC experiments confirm our conventional flow cytometry and confocal microscopy findings that

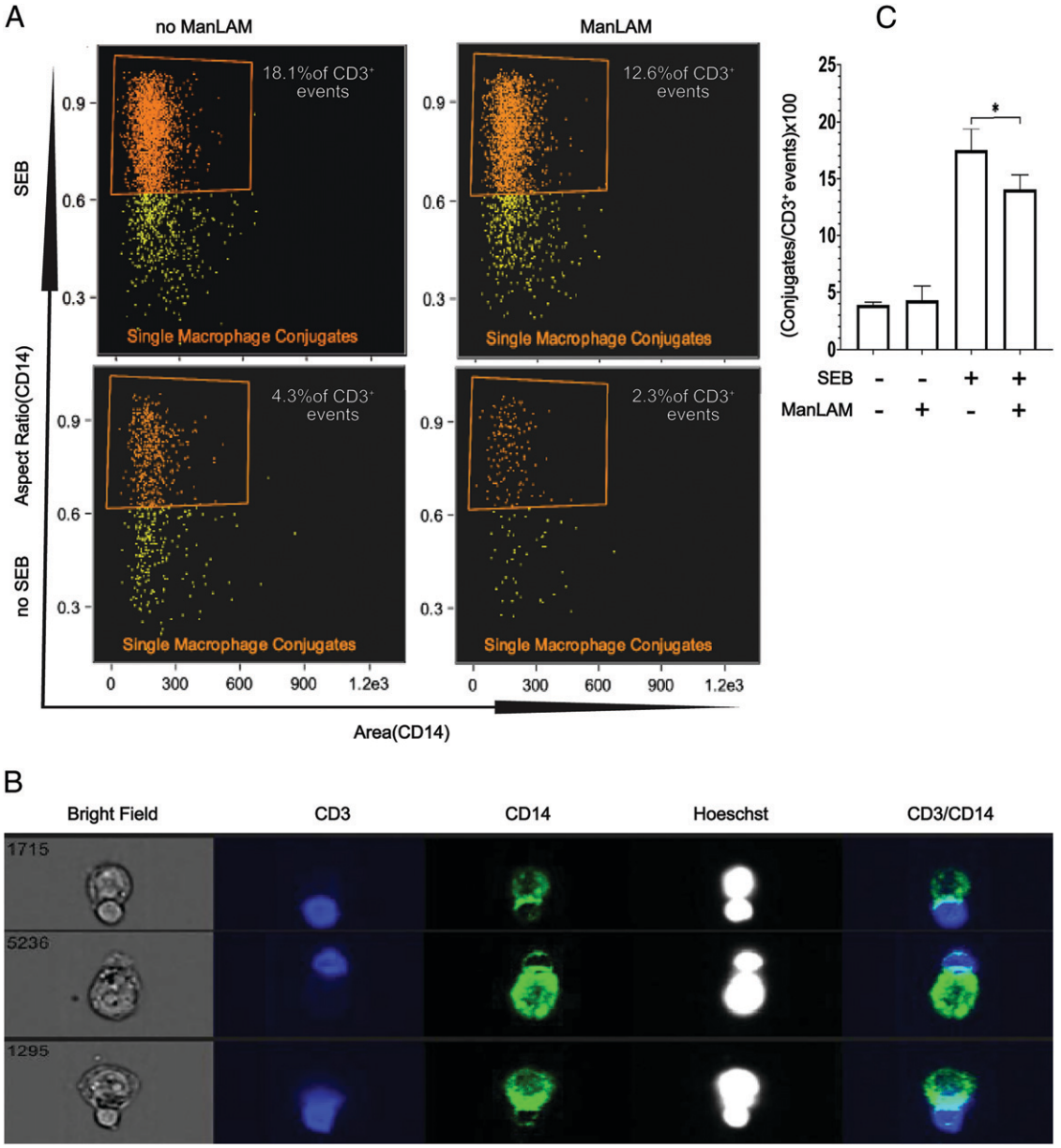

FIGURE 4. By IFC, ManLAM reduces the number of conjugates formed between $CD4^+$ T cells and THP-1 cells. Purified human $CD4^+$ T cells were incubated with or without ManLAM (40 μg/ml) for 1 h. THP-1 cells were loaded with SEB (5 μg/ml) for 30 min. Cells were washed and resuspended at 50,000 cells/μl in RPMI 1640 supplemented with 6 mM calcium chloride. $CD4^+$ T cells and THP-1 cells were cocultured at 1:1 ratio for 30 min at 37°C in 5% CO_2. Cocultured cells were fixed and stained for CD3 and CD14 for 40 min on ice. A drop of Hoechst (DAPI) dye was added to each sample before acquisition. Samples were acquired on Amnis ImageStream imaging flow cytometer at 40× magnification at low-flow rate using INSPIRE software and analyzed using IDEAS software. Approximately 30,000 events were acquired and analyzed per sample. A conjugate was defined as an event imaged by bright field that was also positive for Hoechst dye and CD3 and CD14 with an aspect ratio ≥ 0.6 for both CD3 and CD14 masks; i.e., only conjugates of single $CD4^+$ T cells and THP-1 cells were included in the analysis. (**A**) Representative dot plots of conjugates as a percentage of total gated $CD3^+$ events from one of four experiments from two donors. (**B**) Representative IFC images showing conjugates from one of four experiments from two donors. (**C**) Summary results for four experiments from two donors presented as percentage of conjugates formed across the different experimental conditions (mean ± SEM, paired *t* test, $*p \leq 0.05$).

$CD4^+$ T cells treated with ManLAM form fewer conjugates compared with ManLAM nontreated T cells.

ManLAM reduces the localization of LCK toward the $CD4^+$ T cell–macrophage synapse as measured by IFC

In addition to counting true conjugates, IFC allows assessment of the quality of the activation interface between SEB-loaded APCs and $CD4^+$ T cells, allowing us to use LCK localization to the IS as a measure of $CD4^+$ T cell activation. As shown in Fig. 5A, we measured LCK localization to the IS using a valley mask between the two nuclei of $CD4^+$ T cell and THP-1 cell that were forming a conjugate. The localization of LCK to IS can be measured by both LCK redistribution (i.e., % of LCK in valley mask compared with total cellular LCK) and the brightness of LCK (maximum pixel) in the valley mask compared with the mean brightness (mean pixel) of LCK over the entire conjugate (Fig. 5B). With ManLAM-treated $CD4^+$ T cells, we find that there is approximately a 24% reduction in $CD4^+$ T cells that form conjugates with at least 20% of LCK within the IS compared with ManLAM untreated T cells (Fig. 5C–E). Overall, these experiments demonstrate that ManLAM pretreatment not

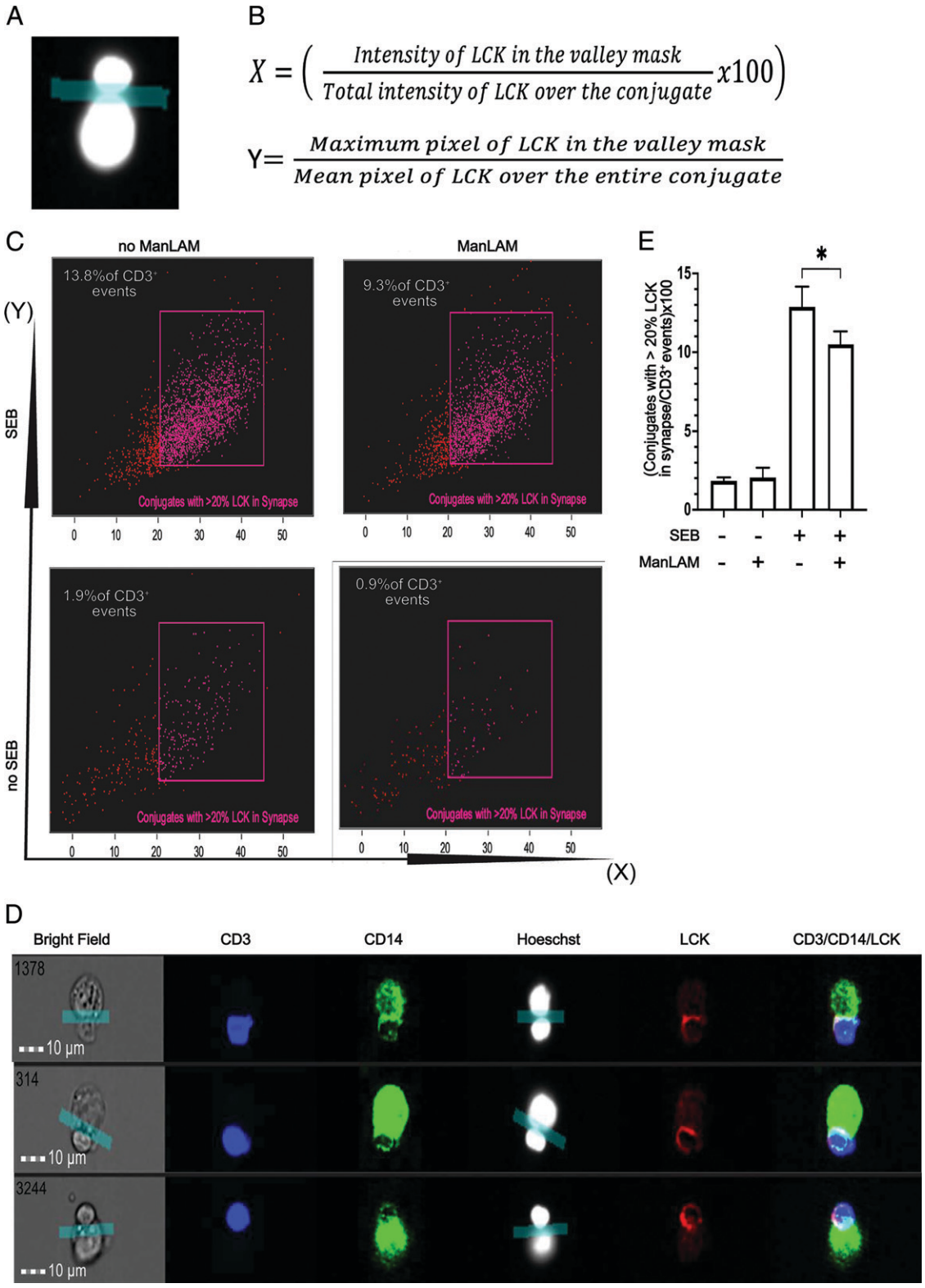

FIGURE 5. Exposure to ManLAM reduces the percentage of conjugates with at least 20% of total LCK in the IS of $CD4^+$ T cells and THP-1 cells. Human $CD4^+$ T cells were incubated with or without ManLAM (40 µg/ml) for 1 h, and THP-1 cells were treated with SEB (5 µg/ml), then cocultured, stained for CD3, CD14, and LCK, and acquired as described in Fig. 4. (**A**) An IS was defined by applying the valley mask feature of IDEAS software to the interface of the Hoechst dye–stained nuclei of $CD3^+$ and $CD14^+$ cells as shown in representative image from one of four experiments from two donors. (**B**) Two parameters were used to measure LCK translocation to the IS: (1) redistribution of LCK (as % of total cellular LCK) to the IS in the valley mask, and (2) the ratio of maximum brightness (maximum pixel) of LCK in the IS to the mean brightness (mean pixel) of LCK over the entire cell. (**C**) IFC dot plots for conjugates with at least 20% of LCK in the IS as a percentage of total $CD3^+$ events gated when the parameters described in (B) were applied. Representative dot plots of one experiment of four from two donors are shown. (**D**) IFC images showing translocation of LCK to the IS. Representative images of one experiment of four from two donors are shown. (**E**) Summary data from four experiments from two independent donors of $CD4^+$ T cells (mean ± SEM, paired *t* test, $*p \leq 0.05$).

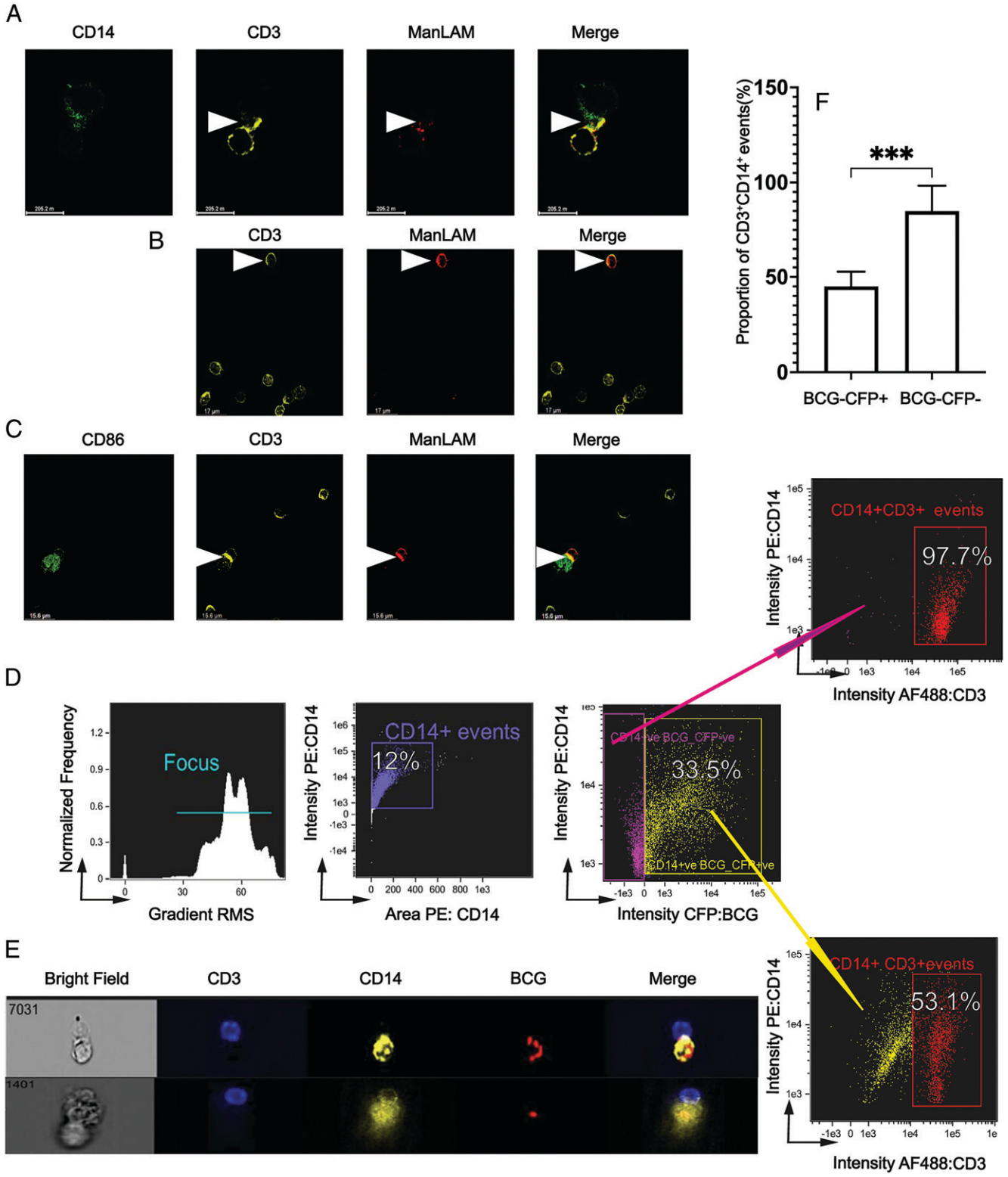

FIGURE 6. ManLAM is transferred from BCG-infected monocytes to $CD4^+$ T cells, localizes to the IS, and reduces conjugate formation of $CD4^+$ T cells with infected monocytes. (**A**) ManLAM localizes to the IS as determined by confocal microscopy. Purified human $CD4^+$ T cells were incubated with ManLAM (40 μg/ml) for 1 h and cocultured at 1:1 with THP-1 cells loaded with SEB (5 μg/ml) for 30 min. Cocultured cells were layered on glass slides and incubated for 15 min and then stained for CD3, CD14, and ManLAM for 3 h followed by respective secondary Abs for 1 h. Slides were imaged under 60× oil immersion. Representative confocal microscopy images from one of two experiments from two donors are shown with ManLAM localizing to the synapse (white arrow). (**B**) ManLAM is transferred to $CD4^+$ T cells by BCG-infected monocytes. Primary monocytes were infected with BCG for 48 h at MOI 5:1 before addition of autologous $CD4^+$ T cells. $CD4^+$ T cells and BCG-infected monocytes were cocultured for 72 h. Cocultures were then layered on glass slides and incubated for 15 min and then stained with rabbit anti-CD3 and human anti-LAM (L1AM04) for 3 h followed by the respective secondary Abs for 1 h. Slides were imaged under 60× oil immersion. Representative confocal microscopy images from one of three experiments from three donors showing ManLAM staining of $CD4^+$ T cells (white arrow) are shown. (**C**) ManLAM localizes to the IS when $CD4^+$ T cells are cocultured with BCG-infected monocytes. Primary monocytes were infected with BCG at MOI 5:1 for 48 h and cocultured with autologous $CD4^+$ T cells as in (B). *(Figure legend continues)*

only reduced conjugate formation but also impacted the activation and LCK translocation in $CD4^+$ T cells that were able to form conjugates.

ManLAM colocalizes with $CD4^+$ T cells cocultured with BCG-infected monocytes, and $CD4^+$ T cells form fewer conjugates with infected versus noninfected monocytes

Our previous studies demonstrated that ManLAM and other glycolipids can be released in the form of bacterial microvesicles by macrophages infected with mycobacteria (16, 19). Thus, we sought to determine the extent to which ManLAM from human monocytes infected with BCG colocalizes with human $CD4^+$ T cells and the impact of BCG infection on the IS. Primary human $CD4^+$ T cells were cocultured with autologous mononuclear phagocytes. We also took advantage of recently developed high-affinity human anti-ManLAM mAb L1AM04 to detect ManLAM in $CD4^+$ T cells (21). Using mAb L1AM04, we directly identified ManLAM in the membrane of ManLAM-pretreated $CD4^+$ T cells (Supplemental Fig. 1). In some $CD4^+$ T cells, we identified increased amounts of ManLAM directly in the IS with SEB-pretreated macrophages (Fig. 6A).

We next determined whether ManLAM can be acquired by $CD4^+$ T cells cocultured with BCG-infected monocytes, and the ability of infected monocytes to form conjugates. Primary monocytes were infected with wild-type BCG and cocultured with autologous $CD4^+$ T cells for 72 h before adding SEB for 1 h and processing cells for confocal imaging. Confocal images of $CD4^+$ T cells cocultured with monocytes infected with wild-type BCG at MOI 5:1 demonstrate the transfer of ManLAM from infected monocytes to $CD4^+$ T cells (Fig. 6B) with a suggestion in some images of increased ManLAM in the IS with monocytes (Fig. 6C). IFC was used to quantify the ability of BCG-infected monocytes to form conjugates with $CD4^+$ T cells. At MOI 1:1, BCG-infected monocytes formed 50% fewer conjugates with $CD4^+$ T cells than uninfected monocytes (Fig. 6D–F). Thus, BCG-infected monocytes can transfer ManLAM to $CD4^+$ T cells, resulting in less efficient conjugate formation.

Discussion

Our results demonstrate the ability of *M. tuberculosis*'s major cell-wall glycolipid, ManLAM, to inhibit human $CD4^+$ T cell activation in three areas. First, we extended our functional observations from murine studies to primary human $CD4^+$ T cells. Second, we explored the impact of ManLAM on the formation of the IS between human $CD4^+$ T cells and macrophages, and LCK migration toward the IS. Third, we determined ManLAM's transfer from BCG-infected human macrophages to $CD4^+$ T cells and the impact of BCG infection on the IS.

ManLAM inhibited the production of IL-2, TNF-α, and IFN-γ and expression of CD25 without significantly changing the expression of CD69. Expression of inhibitory receptors CTLA-4, PD-1, TIM-3, and Lag-3, or costimulatory molecules CD40L and ICOS was not affected by ManLAM. These findings extended earlier findings with murine to human $CD4^+$ T cells that the mechanism of ManLAM-induced T cell hyporesponsiveness is distinct from disturbing the balance of costimulatory and inhibitory receptor signaling (17). The absence of inhibitory molecule upregulation or downregulation of CD69 argues against induction of $CD4^+$ T cell exhaustion (29). Suppression of CD25 expression supports disruption of the TCR/IL-2R signaling axis because of ManLAM's capacity to inhibit TCR signaling by insertion in CD3/TCR-containing lipid rafts, which in turn impacts IS formation (17).

Because professional APCs are important for $CD4^+$ T cell responses to *M. tuberculosis* bacilli and their Ags, and mononuclear phagocytes are a niche for *M. tuberculosis* growth, we focused on the T cell–macrophage IS. We first evaluated conjugate formation between primary $CD4^+$ T cells and THP-1 macrophages using conventional flow cytometry. ManLAM-exposed $CD4^+$ T cells formed fewer conjugates with THP-1 macrophages when SEB was used to cross-link TCR with MHC-II on macrophages. IFC provided higher analytical stringency for conjugate enumeration by focusing on individual $CD4^+$ T cell–macrophage conjugates, in addition to allowing analysis of larger numbers of individual events (26–28). IFC confirmed that ManLAM exposure reduced macrophage–T cell conjugates but less significantly: 40% by conventional flow cytometry versus 20% reduction by IFC.

IFC, aside from detecting conjugates, also allowed measurement of LCK localization to the T-cell–macrophage interface of successful conjugates. LCK, a Src kinase, is mobilized to the IS by CD4 (and CD8) coreceptors upon T cell–APC engagement (30–32). LCK phosphorylates ITAMs on CD3ε (33, 34). ZAP70 kinase docks to phosphorylated CD3ε ITAMs and is then phosphorylated by LCK (33, 34). Thus, mobilization of LCK toward the IS is essential for T cell activation through the TCR–CD3 complex. Our previous studies showed that *M. tuberculosis*–derived glycolipids, including ManLAM, block phosphorylation of ZAP70 and adaptor protein LAT (20, 35). IFC showed that ManLAM-exposed $CD4^+$ T cells that did form conjugates had reduced localization of LCK to the IS, measured both by the percentage of total LCK found in the IS and the brightness of LCK signal in the IS. Thus, IFC determined that ManLAM exposure not only subtly reduced the number of $CD4^+$ T cell–macrophage conjugates, but that when conjugates were formed there was a reduction in LCK localization to the IS. Confocal microscopy of anti-CD3–coated slides as pseudo-APC confirmed that ManLAM reduced LCK mobilization toward the activation interface. Thus, complementary experimental approaches demonstrate the impact of ManLAM exposure on IS formation between monocytes and primary human $CD4^+$ T cells. Combining modestly reduced conjugate formation with modestly reduced suboptimal LCK localization is likely additive and together provide a mechanism for substantial ManLAM-mediated inhibition of $CD4^+$ T cell activation.

ManLAM can be readily detected in *M. tuberculosis*–infected tissues in animal models; clinically, ManLAM is found in the urine, sputum, and serum of persons with advanced TB and remains a target for new TB diagnostics in pediatric and HIV-TB (21, 22, 36, 37). Recent

Afterward, SEB was added for 1 h. Cocultures were layered on glass slides and incubated for 15 min and then stained with rabbit anti-CD3, mouse anti-CD86, and human anti-LAM (L1AM04) for 3 h followed by the respective secondary Abs for 1 h. Slides were imaged under 60× oil immersion. Representative confocal microscopy images from one of three experiments from three donors showing ManLAM localizing to the IS of $CD4^+$ T cells cocultured with BCG-infected monocytes (white arrow) are shown. (**D**–**F**) BCG infection reduces $CD4^+$ T cell–monocyte conjugate formation. Primary monocytes were infected with CFP-BCG for 48 h at MOI 1:1 before addition of autologous $CD4^+$ T cells. $CD4^+$ T cells and BCG-infected monocytes were cocultured for 72 h. Then SEB was added for 1 h. Cocultured cells were stained with AF488-conjugated anti-CD3 and PE-conjugated anti-CD14 mAbs and acquired for IFC on ImageStream imaging flow cytometer. (D) IFC gating strategy in which two populations of $CD14^+$ events were defined: $CD14^+BCG/CFP^+$ (infected) and $CD14^+BCG/CFP^-$ (noninfected). Representative IFC dot plots from one experiment of three from three donors are shown. (E) Images of $CD4^+$ T cell–monocyte conjugates with infected monocytes ($CD3^+CD14^+BCG/CFP^+$). Representative images from one experiment of three from three donors are shown. (F) Summary percentages of three experiments from three donors showing BCG-infected versus BCG-uninfected monocytes that form conjugates with $CD4^+$ T cells (***$p \leq 0.001$).

studies show that *M. tuberculosis* and other mycobacteria produce bacterial microvesicles that can be released directly or their molecules incorporated into exosomes by infected macrophages (16, 19). Thus, ManLAM and other glycolipids are readily found in the microenvironment of *M. tuberculosis*–infected cells and tissues (19). It should be noted that although this study focuses on ManLAM, the major glycolipid, its precursors phosphatidylinostol mannosides and lipomannan also have T cell–inhibitory activity (19). The availability of newer and more sensitive mAbs for ManLAM and its components allowed us to extend our studies to the direct transfer of ManLAM from infected macrophages to $CD4^+$ T cells (21, 22). Confocal microscopy showed ManLAM transfer from BCG-infected macrophages to $CD4^+$ T cells and colocalization to the IS. Interestingly, both conjoined and nonconjoined $CD4^+$ T cells stained positive for ManLAM when cultured with BCG-infected macrophages, indicating that direct contact is not required for ManLAM to reach T cells. However, when $CD4^+$ T cells were cocultured with a mixture of BCG-infected and uninfected macrophages, that proximity to the source of ManLAM mattered.

Our studies have some limitations. First, *M. bovis* BCG is not identical to *M. tuberculosis*, although they share the same ManLAM precursors and ManLAM. All ManLAM experiments were with ManLAM purified from *M. tuberculosis*. Second, it is possible that naive and memory $CD4^+$ T cells differ in sensitivity to the inhibitory activity of ManLAM. We used purified total $CD4^+$ T cells, which contain cells of both phenotypes. The focus of our studies was on the interaction of $CD4^+$ T cells with macrophages, which in the context of *M. tuberculosis* infection is primarily mediated by memory/effector T cells. Third, the reduction in productive IS formation with $CD4^+$ T cells by BCG-infected macrophages may involve mechanisms in addition to ManLAM transfer. BCG infection might affect the overall efficiency of macrophages to serve as APCs and form productive IS, in addition to ManLAM's effect. Fourth, IFC experiments required large numbers of $CD4^+$ T cells and monocytes for which we used leukapheresis products that limited the number of donors we could use. This may reduce the generalizability of the results. The IFC experiments were critical for extending and gaining insight into how ManLAM interfered with IS integrity and inhibited $CD4^+$ T cell activation. The figure legends for all data shown explicitly state how many experiments were performed and the number of donors used.

Overall, our findings demonstrate ManLAM to likely inhibit activation of T cells by disrupting productive engagement of TCR with the cognate MHC–peptide complex even when presented by a competent APC. Suboptimal activation may render $CD4^+$ T cells anergic and/or hypofunctional. In earlier studies, ManLAM-exposed murine $CD4^+$ T cells were found to become anergic and expressed increased Gene Related to Anergy in Lymphocytes. This hypofunctional state persisted even when the glycolipid was cleared from the T cell plasma membrane (17). Anergy is associated with upregulation of other E3 ligases such as Cbl-b and Itch that target proximal TCR signaling molecules (e.g., LCK, ZAP70, and LAT) for proteasomal degradation (38–42). Anergy can result from poor T cell–APC engagement, such as suboptimal IS formation.

Secretion of mycobacterial glycolipids such as ManLAM by *M. tuberculosis*–infected macrophages may result in poor engagement of $CD4^+$ T cells and possibly anergy as a result of suboptimal IS formation and CD3/TCR signaling. This provides *M. tuberculosis* a mechanism for evasion of T cell recognition and enhances its survival in its infectious niche: the macrophage.

Acknowledgments

We thank Scott Reba for technical assistance. We are grateful to Case Western Reserve University Light Microscopy Imaging Core facility and the Cytometry and Imaging Microscopy of Shared Resource of the Case Comprehensive Cancer Center. We extend our appreciation to Richard DeMarco, the Instrument Field Applications Scientist at Luminex Corporation, for help concerning imaging flow cytometry data analysis.

Disclosures

The authors have no financial conflicts of interest.

References

1. Sia, J. K., and J. Rengarajan. 2019. Immunology of *Mycobacterium tuberculosis* Infections. *Microbiol. Spectr.* 7: 10.1128/microbiolspec.GPP3-0022-2018.
2. Srivastava, S., J. D. Ernst, and L. Desvignes. 2014. Beyond macrophages: the diversity of mononuclear cells in tuberculosis. *Immunol. Rev.* 262: 179–192.
3. Kozakiewicz, L., J. Phuah, J. Flynn, and J. Chan. 2013. The role of B cells and humoral immunity in *Mycobacterium tuberculosis* infection. *Adv. Exp. Med. Biol.* 783: 225–250.
4. Porcelli, S. A., and W. R. Jacobs, Jr. 2019. Exacting Edward Jenner's revenge: the quest for a new tuberculosis vaccine. *Sci. Transl. Med.* 11: eaax4219.
5. Harding, C. V., and W. H. Boom. 2010. Regulation of antigen presentation by *Mycobacterium tuberculosis*: a role for Toll-like receptors. *Nat. Rev. Microbiol.* 8: 296–307.
6. Prezzemolo, T., G. Guggino, M. P. La Manna, D. Di Liberto, F. Dieli, and N. Caccamo. 2014. Functional signatures of human CD4 and CD8 T cell responses to *Mycobacterium tuberculosis*. *Front. Immunol.* 5: 180.
7. World Health Organization. 2018. Global *Tuberculosis Report* 2018. Geneva: World Health Organization. Available at: https://apps.who.int/iris/handle/10665/274453.
8. Boom, W. H., U. E. Schaible, and J. M. Achkar. 2021. The knowns and unknowns of latent *Mycobacterium tuberculosis* infection. *J. Clin. Invest.* 131: e136222.
9. Jasenosky, L. D., T. J. Scriba, W. A. Hanekom, and A. E. Goldfeld. 2015. T cells and adaptive immunity to *Mycobacterium tuberculosis* in humans. *Immunol. Rev.* 264: 74–87.
10. Mayer-Barber, K. D., and D. L. Barber. 2015. Innate and adaptive cellular immune responses to *Mycobacterium tuberculosis* infection. *Cold Spring Harb. Perspect. Med.* 5: a018424.
11. Harari, A., V. Rozot, F. Bellutti Enders, M. Perreau, J. M. Stalder, L. P. Nicod, M. Cavassini, T. Calandra, C. L. Blanchet, K. Jaton, et al. 2011. Dominant TNF-α+ *Mycobacterium tuberculosis*-specific CD4+ T cell responses discriminate between latent infection and active disease. *Nat. Med.* 17: 372–376.
12. Lindestam Arlehamn, C. S., A. Gerasimova, F. Mele, R. Henderson, J. Swann, J. A. Greenbaum, Y. Kim, J. Sidney, E. A. James, R. Taplitz, et al. 2013. Memory T cells in latent *Mycobacterium tuberculosis* infection are directed against three antigenic islands and largely contained in a CXCR3+CCR6+ Th1 subset. *PLoS Pathog.* 9: e1003130.
13. Weiss, G., and U. E. Schaible. 2015. Macrophage defense mechanisms against intracellular bacteria. *Immunol. Rev.* 264: 182–203.
14. Portal-Celhay, C., J. M. Tufariello, S. Srivastava, A. Zahra, T. Klevorn, P. S. Grace, A. Mehra, H. S. Park, J. D. Ernst, W. R. Jacobs, Jr., and J. A. Philips. 2016. *Mycobacterium tuberculosis* EsxH inhibits ESCRT-dependent $CD4^+$ T-cell activation. *Nat. Microbiol.* 2: 16232.
15. Srivastava, S., P. S. Grace, and J. D. Ernst. 2016. Antigen export reduces antigen presentation and limits T cell control of *M. tuberculosis*. *Cell Host Microbe* 19: 44–54.
16. Athman, J. J., Y. Wang, D. J. McDonald, W. H. Boom, C. V. Harding, and P. A. Wearsch. 2015. Bacterial membrane vesicles mediate the release of *Mycobacterium tuberculosis* lipoglycans and lipoproteins from infected macrophages. *J. Immunol.* 195: 1044–1053.
17. Sande, O. J., A. F. Karim, Q. Li, X. Ding, C. V. Harding, R. E. Rojas, and W. H. Boom. 2016. Mannose-capped lipoarabinomannan from *Mycobacterium tuberculosis* induces CD4+ T cell anergy via GRAIL. *J. Immunol.* 196: 691–702.
18. Prados-Rosales, R., A. Baena, L. R. Martinez, J. Luque-Garcia, R. Kalscheuer, U. Veeraraghavan, C. Camara, J. D. Nosanchuk, G. S. Besra, B. Chen, et al. 2011. Mycobacteria release active membrane vesicles that modulate immune responses in a TLR2-dependent manner in mice. *J. Clin. Invest.* 121: 1471–1483.
19. Athman, J. J., O. J. Sande, S. G. Groft, S. M. Reba, N. Nagy, P. A. Wearsch, E. T. Richardson, R. Rojas, W. H. Boom, S. Shukla, and C. V. Harding. 2017. *Mycobacterium tuberculosis* membrane vesicles inhibit T cell activation. *J. Immunol.* 198: 2028–2037.
20. Mahon, R. N., R. E. Rojas, S. A. Fulton, J. L. Franko, C. V. Harding, and W. H. Boom. 2009. *Mycobacterium tuberculosis* cell wall glycolipids directly inhibit CD4+ T-cell activation by interfering with proximal T-cell-receptor signaling. *Infect. Immun.* 77: 4574–4583.
21. Ishida, E., D. T. Corrigan, R. J. Malonis, D. Hofmann, T. Chen, A. G. Amin, D. Chatterjee, M. Joe, T. L. Lowary, J. R. Lai, and J. M. Achkar. 2021. Monoclonal antibodies from humans with *Mycobacterium tuberculosis* exposure or latent infection recognize distinct arabinomannan epitopes. *Commun. Biol.* 4: 1181.
22. Corrigan, D. T., E. Ishida, D. Chatterjee, T. L. Lowary, and J. M. Achkar. 2023. Monoclonal antibodies to lipoarabinomannan/arabinomannan—characteristics and implications for tuberculosis research and diagnostics. *Trends Microbiol.* 31: 22–35.
23. Li, Q., A. F. Karim, X. Ding, B. Das, C. Dobrowolski, R. M. Gibson, M. E. Quiñones-Mateu, J. Karn, and R. E. Rojas. 2016. Novel high throughput pooled shRNA

screening identifies NQO1 as a potential drug target for host directed therapy for tuberculosis. *Sci. Rep.* 6: 27566.
24. Valdivia, R. H., A. E. Hromockyj, D. Monack, L. Ramakrishnan, and S. Falkow. 1996. Applications for green fluorescent protein (GFP) in the study of host-pathogen interactions. *Gene* 173: 47–52.
25. Pecora, N. D., S. A. Fulton, S. M. Reba, M. G. Drage, D. P. Simmons, N. J. Urankar-Nagy, W. H. Boom, and C. V. Harding. 2009. *Mycobacterium* bovis BCG decreases MHC-II expression in vivo on murine lung macrophages and dendritic cells during aerosol infection. *Cell. Immunol.* 254: 94–104.
26. Barteneva, N. S., E. Fasler-Kan, and I. A. Vorobjev. 2012. Imaging flow cytometry: coping with heterogeneity in biological systems. *J. Histochem. Cytochem.* 60: 723–733.
27. Payes, C. A. J., S. Friend, and G. Helguer. 2012. Cell interaction analysis by imaging flow cytometry. *Cell Interaction. InTech.* Available at: http://dx.doi.org/10.5772/51147.
28. Ahmed, F., S. Friend, T. C. George, N. Barteneva, and J. Lieberman. 2009. Numbers matter: quantitative and dynamic analysis of the formation of an immunological synapse using imaging flow cytometry. *J. Immunol. Methods* 347: 79–86.
29. Crespo, J., H. Sun, T. H. Welling, Z. Tian, and W. Zou. 2013. T cell anergy, exhaustion, senescence, and stemness in the tumor microenvironment. *Curr. Opin. Immunol.* 25: 214–221.
30. Barber, E. K., J. D. Dasgupta, S. F. Schlossman, J. M. Trevillyan, and C. E. Rudd. 1989. The CD4 and CD8 antigens are coupled to a protein-tyrosine kinase (p56lck) that phosphorylates the CD3 complex. *Proc. Natl. Acad. Sci. USA* 86: 3277–3281.
31. Rudd, C. E., J. M. Trevillyan, J. D. Dasgupta, L. L. Wong, and S. F. Schlossman. 1988. The CD4 receptor is complexed in detergent lysates to a protein-tyrosine kinase (pp58) from human T lymphocytes. *Proc. Natl. Acad. Sci. USA* 85: 5190–5194.
32. Filipp, D., J. Zhang, B. L. Leung, A. Shaw, S. D. Levin, A. Veillette, and M. Julius. 2003. Regulation of Fyn through translocation of activated Lck into lipid rafts. *J. Exp. Med.* 197: 1221–1227.
33. Huse, M. 2009. The T-cell-receptor signaling network. *J. Cell Sci.* 122: 1269–1273.
34. Au-Yeung, B. B., S. Deindl, L. Y. Hsu, E. H. Palacios, S. E. Levin, J. Kuriyan, and A. Weiss. 2009. The structure, regulation, and function of ZAP-70. *Immunol. Rev.* 228: 41–57.
35. Mahon, R. N., O. J. Sande, R. E. Rojas, A. D. Levine, C. V. Harding, and W. H. Boom. 2012. *Mycobacterium tuberculosis* ManLAM inhibits T-cell-receptor signaling by interference with ZAP-70, Lck and LAT phosphorylation. *Cell. Immunol.* 275: 98–105.
36. Conesa-Botella, A., M. M. Loembé, Y. C. Manabe, W. Worodria, D. Mazakpwe, K. Luzinda, H. Mayanja-Kizza, M. Miri, O. Mbabazi, O. Koole, et al.; TB IRIS Group. 2011. Urinary lipoarabinomannan as predictor for the tuberculosis immune reconstitution inflammatory syndrome. *J. Acquir. Immune Defic. Syndr.* 58: 463–468.
37. Choudhary, A., D. Patel, W. Honnen, Z. Lai, R. S. Prattipati, R. B. Zheng, Y.-C. Hsueh, M. L. Gennaro, A. Lardizabal, B. I. Restrepo, et al. 2018. Characterization of the antigenic heterogeneity of lipoarabinomannan, the major surface glycolipid of *Mycobacterium tuberculosis*, and complexity of antibody specificities toward this antigen. *J. Immunol.* 200: 3053–3066.
38. Tang, R., W. Y. Langdon, and J. Zhang. 2019. Regulation of immune responses by E3 ubiquitin ligase Cbl-b. *Cell. Immunol.* 340: 103878.
39. Schmidt, M. H. H., and I. Dikic. 2005. The Cbl interactome and its functions. *Nat. Rev. Mol. Cell Biol.* 6: 907–918.
40. Doherty, M., D. G. Osborne, D. L. Browning, D. C. Parker, and S. A. Wetzel. 2010. Anergic CD4+ T cells form mature immunological synapses with enhanced accumulation of c-Cbl and Cbl-b. *J. Immunol.* 184: 3598–3608.
41. Mueller, D. L. 2004. E3 ubiquitin ligases as T cell anergy factors. *Nat. Immunol.* 5: 883–890.
42. Park, Y., H.-S. Jin, D. Aki, J. Lee, and Y.-C. Liu. 2014. The ubiquitin system in immune regulation. *Adv. Immunol.* 124: 17–66.